

Hierarchical fractional-step approximations and parallel kinetic Monte Carlo algorithms

Giorgos Arampatzis^a, Markos A. Katsoulakis^{b,*}, Petr Plecháč^d, Michela Taufer¹, Lifan Xu¹

^a*Department of Applied Mathematics, University of Crete and Foundation of Research and Technology-Hellas, Greece*

^b*Department of Mathematics and Statistics, University of Massachusetts at Amherst, Amherst, MA 01003, USA*

^c*Department of Mathematical Sciences, University of Delaware, Newark, DE 19716, USA*

^d*Department of Computer Science, University of Delaware, Newark, DE 19716, USA*

Abstract

We present a mathematical framework for constructing and analyzing parallel algorithms for lattice Kinetic Monte Carlo (KMC) simulations. The resulting algorithms have the capacity to simulate a wide range of spatio-temporal scales in spatially distributed, non-equilibrium physiochemical processes with complex chemistry and transport micro-mechanisms. The algorithms can be tailored to specific hierarchical parallel architectures such as multi-core processors or clusters of Graphical Processing Units (GPUs). The proposed parallel algorithms are controlled-error approximations of kinetic Monte Carlo algorithms, departing from the predominant paradigm of creating parallel KMC algorithms with exactly the same master equation as the serial one.

Our methodology relies on a spatial decomposition of the Markov operator underlying the KMC algorithm into a hierarchy of operators corresponding to the processors' structure in the parallel architecture. Based on this operator decomposition, we formulate *Fractional Step Approximation schemes* by employing the Trotter Theorem and its random variants; these schemes, (a) determine the *communication schedule* between processors, and (b) are run independently on each processor through a serial KMC simulation, called a *kernel*, on each fractional step time-window.

Furthermore, the proposed mathematical framework allows us to rigorously justify the numerical and statistical consistency of the proposed algorithms, showing the convergence of our approximating schemes to the original serial KMC. The approach also provides a systematic evaluation of different processor communicating schedules. We carry out a detailed benchmarking of the parallel KMC schemes using available exact solutions, for example, in Ising-type systems

*Corresponding author

Email addresses: garab@math.uoc.gr (Giorgos Arampatzis), markos@math.umass.edu (Markos A. Katsoulakis), plechac@math.udel.edu (Petr Plecháč), taufer@cis.udel.edu (Michela Taufer), xulifan@udel.edu (Lifan Xu)

and we demonstrate the capabilities of the method to simulate complex spatially distributed reactions at very large scales on GPUs. Finally, we discuss *work load balancing* between processors and propose a re-balancing scheme based on probabilistic mass transport methods.

Keywords: Kinetic Monte Carlo method, Parallel Algorithms, Markov semigroups, Operator Splitting, Graphical Processing Unit (GPU)

1. Introduction

Kinetic Monte Carlo algorithms have proved to be an important tool for the simulation of out-of-equilibrium, spatially distributed processes. Such models arise in physiochemical applications ranging from materials science and catalysis, to complex biological processes. Typically the simulated models involve chemistry and/or transport micro-mechanisms for atoms and molecules, e.g., reactions, adsorption, desorption processes and diffusion on surfaces and through complex media, [19, 3, 7]. Furthermore, mathematically similar mechanisms and corresponding Kinetic Monte Carlo simulations arise in agent-based, evolutionary games problems in epidemiology, ecology and traffic networks, [35].

The simulation of stochastic lattice systems using Kinetic Monte Carlo (KMC) methods relies on the direct numerical simulation of the underlying Continuous Time Markov Chain (CTMC). Since such stochastic processes are set on a lattice (square, hexagonal, etc.) Λ_N with N sites, they have a discrete, albeit high-dimensional, configuration space Σ and necessarily have to be of jump type describing transitions between different configurations $\sigma \in \Sigma$. Mathematically, CTMC are defined in terms of the transition rates $c(x, \omega; \sigma)$ which correspond to an updating micro-mechanism that describes completely the evolution of the stochastic process as a transition from a current configuration σ of the system to a new configuration $\sigma^{x, \omega}$ by performing an update in a neighborhood of the site $x \in \Lambda_N$. In other words the probability of a transition over an infinitesimal time interval δt is $\mathbb{P}(S_{t+\delta t} = \sigma^{x, \omega} | S_t = \sigma) = c(x, \omega; \sigma)\delta t + o(\delta t^2)$. In turn, the transition rates define the total rate

$$\lambda(\sigma) = \sum_{x \in \Lambda_N} \sum_{\omega \in \mathcal{S}_x} c(x, \omega; \sigma), \quad (1)$$

which is the intensity of the exponential waiting time for a jump to be performed when the system is currently at the state σ . Here $\omega \in \mathcal{S}_x$, where \mathcal{S}_x is the set of all possible configurations that correspond to an update at a neighborhood Ω_x of the site x . Once this exponential “clock” signals a jump, then the system transitions from the state σ to a new configuration $\sigma^{x, \omega}$ with probability

$$p(\sigma, \sigma^{x, \omega}) = \frac{c(x, \omega; \sigma)}{\lambda(\sigma)}. \quad (2)$$

Thus the full stochastic evolution is completely defined. We refer to the discussion in Section 2 for a complete mathematical description of the KMC method.

The implementation of this method is based on efficient calculation of (1) and (2), and was first developed in [6], known as a BKL Algorithm, for stochastic lattice Ising models, and in [11] known as Stochastic Simulation Algorithm (SSA) for reaction systems. However, as it is evident from formulas (1) and (2), the algorithms are inherently serial as updates are done at one site $x \in \Lambda_N$ at a time, while on the other hand the calculation of (1) depends on information from the entire spatial domain Λ_N . For these reasons it seems, at first glance, that KMC algorithms cannot be parallelized easily.

However, Lubachevsky, in [22], proposed an *asynchronous* approach for parallel KMC simulation in the context of Ising systems, in the sense that different processors simulate independently parts of the physical domain, while inconsistencies at the boundaries are corrected with a series of suitable rollbacks. This method relies on uniformization of the total rates over each processor, see also [13] for the use of uniformization in the parallel simulation of general CTMC. Thus the approach yields a *null-event* algorithm, [19], which includes rejected moves over the entire domain of each processor. Furthermore, Lubachevsky proposed a modification in order to incorporate the BKL Algorithm in his parallelization method, which was implemented and tested in [17]. This is a partially rejection-free (still asynchronous) algorithm, where BKL-type rejection-free simulations are carried out in the interior of each processor, while uniform rates were used at the boundary, reducing rejections over just the boundary set. However, in spite of the proposed improvements, these asynchronous algorithms may still have a high number of rejections for boundary events and rollbacks, which considerably reduce the parallel efficiency, [33]. Advancing processors in time in a synchronous manner over a fixed time-window can provide a way to mitigate the excessive number of boundary inconsistencies between processors and ensuing rejections and rollbacks in earlier methods. Such *synchronous* parallel KMC algorithms were proposed and extensively studied in [9, 33, 25, 28]. However, several costly global communications are required at each cycle between all processors, whenever a boundary event occurs in any one of them, in order to avoid errors in the inter-processor communication and rollbacks, [28].

As we will discuss further in this paper, many of the challenges in parallel KMC can be addressed by abandoning the earlier perspective on creating a parallel KMC algorithm with the exactly same rates (and hence the generator and master equation) as the serial algorithm, see [24] for a discussion on exact algorithms. This is a very natural idea in the numerical analysis of continuum models such as Ordinary and Partial Differential Equations (ODE/PDE). First, in [34] the authors propose an *approximate* algorithm, in order to create a parallelization scheme for KMC. It was recently demonstrated [28, 4], that this method is very promising: boundary inconsistencies are resolved in a straightforward fashion, while there is an absence of global communications in contrast to synchronous relaxation schemes discussed earlier. Finally, we note that, among the parallel algorithms tested in [28], the approximate algorithm had the highest parallel efficiency.

Here we develop a general mathematical framework for *parallelizable approximations* of the KMC algorithm. Our approach relies on first developing a

spatial decomposition of the Markov operator, that defines the Kinetic Monte Carlo algorithm, into a hierarchy of operators. The decomposition is tailored to the processor architecture. Based on this operator decomposition, we formulate *Fractional Step Approximation* schemes by employing the Trotter product formula. In turn these approximating schemes determine *Communication Schedule* between processors through the sequential application of the operators in the decomposition, and the time step employed in the particular fractional step scheme. Here we discuss deterministic schedules resulting from Lie- and Strang-type fractional step schemes, as well as random schedules derived by the Random Trotter Theorem, [18]. We show that the scheme in [34] is a particular case of a random schedule and can be mathematically analyzed within the proposed framework. We recall that the deterministic Trotter Theorem was first proved in [36] for the approximation of semigroups corresponding to operator sums, and it has found wide application in the numerical ODE/PDE analysis, e.g., [12].

In Section 2 we show that the Fractional Step KMC schemes allow us to run independently on each processor a serial KMC simulation (called a *kernel*) on each fractional time-step window. Furthermore, processor communication is straightforward at the end of each fractional time-step while no global communications or rollbacks are involved. In Section 5 we show that the hierarchical structure of our methodology can be easily implemented for very general physiochemical processes modeled by lattice systems, allowing users to input as the algorithm's KMC kernel their preferred serial algorithm. This flexibility and hierarchical structure are key advantages for tailoring our framework to particular parallel architectures with complex memory and processor hierarchies, e.g., clusters of GPUs.

The proposed mathematical framework allows us to rigorously prove the numerical and statistical consistency of the proposed algorithms, while on the other hand it provides a systematic evaluation of different processor communication schedules. Indeed, in Section 3 the numerical and statistical consistency of the proposed algorithms is rigorously justified by the Trotter Theorem, [36], [12] showing the convergence of our approximating schemes to the original serial KMC algorithm, interpreted as convergence to the underlying Markov operator. Using the Random Trotter Theorem [18] we show that the approximation schemes with a random schedule, including the one in [34] as a special case, are numerically consistent in the approximation limit; that is, as the time step in the fractional step scheme converges to zero, it converges to a continuous time Markov Chain that has the same master equation and generator as the original serial KMC. In Section 4 we show that the proposed mathematical framework can allow the study of controlled-error approximation properties of Fractional Step KMC schemes, as well as the systematic evaluation of different processor communicating schedules, comparing for instance the scheme in [34] to the Lie scheme (12).

Finally, in Section 6 we discuss work-load balancing between processors and propose a re-balancing scheme based on probabilistic mass transport methods, [10], which is particularly well-suited for the proposed fractional step KMC

methods. In Section 7 we present detailed benchmarking of the proposed parallel algorithms using analytically available exact solutions, for instance, in Ising-type systems and demonstrate the capabilities of the method to simulate complex spatially distributed molecular systems, such as CO oxidation on a catalytic surface.

2. Fractional Step Kinetic Monte Carlo Algorithms

We first present the mathematical background of KMC in a more abstract way in order to demonstrate the generality and the applicability of the proposed method. We consider a d -dimensional lattice Λ_N with N lattice sites. We restrict our discussion to lattice gas models where the order parameter or the spin variable takes value in a finite countable set $\Sigma = \{0, 1, \dots, K\}$. At each lattice site $x \in \Lambda_N$ an order parameter (a spin variable) $\sigma(x) \in \Sigma$ is defined. The states in Σ correspond to occupation of the site $x \in \Lambda_N$ by different species. For example, if $\Sigma = \{0, 1\}$ the order parameter models the classical lattice gas with a single species occupying the site x when $\sigma(x) = 1$ and with the site being vacant if $\sigma(x) = 0$. We denote $\{S_t\}_{t \geq 0}$ the stochastic process with values in the configuration space $\mathcal{S} = \Sigma^{\Lambda_N}$.

Our primary focus is on modeling the basic processes of adsorption, desorption, diffusion and reactions between different species. Thus the local dynamics is described by a collection of the transition rates $c(x, \omega; \sigma)$ and by an updating mechanism such that the configuration σ of the system changes into a new configuration $\sigma^{x, \omega}$ by an update in a neighborhood of the site $x \in \Lambda_N$. Here $\omega \in \mathcal{S}_x$, where \mathcal{S}_x is the set of all possible configurations that correspond to an update at a neighborhood Ω_x of the site x . For example, if the modeled process is a diffusion of the classical lattice gas a particle at x , i.e., $\sigma(x)$ can move to any nearest neighbor of x , i.e., $\Omega_x = \{y \in \Lambda_N \mid |x - y| = 1\}$ and \mathcal{S}_x is the set of all possible configurations $\mathcal{S}_x = \Sigma^{\Omega_x}$. In other words the collection of measures $c(x, \omega; \sigma)$ defines the transition probability from σ to $\sigma^{x, \omega}$ over an infinitesimal time interval δt . More precisely, the evolution of the system is described by a continuous time Markov jump process with the generator $\mathcal{L} : C_b(\mathcal{S}) \rightarrow C_b(\mathcal{S})$ acting on continuous bounded test functions $f \in C_b(\mathcal{S})$ according to

$$\mathcal{L}f(\sigma) = \sum_{x \in \Lambda_N} \sum_{\omega \in \mathcal{S}_x} c(x, \omega; \sigma) [f(\sigma^{x, \omega}) - f(\sigma)]. \quad (3)$$

We recall that the evolution of the expected value for an arbitrary observable $f \in C_b(\mathcal{S})$ is given by the action of the Markov semigroup $e^{t\mathcal{L}}$ associated with the generator \mathcal{L} and the process $\{S_t\}_{t \geq 0}$

$$\langle e^{t\mathcal{L}} \mu_0, f \rangle = \mathbb{E}_{S_0} [f(S_t)], \quad (4)$$

where μ_0 is the initial distribution of the process, i.e. of the random variable S_0 , [20]. Practically, the sample paths $\{S_t\}_{t \geq 0}$ are constructed via KMC, that is through the procedure described in (1) and (2).

To elucidate the introduced notation we give a few examples relevant to the processes modeled here. We refer, for instance, to [19, 3, 7] for a complete discussion of the physical processes.

EXAMPLES.

1. *Adsorption/Desorption for single species particles.* In this case spins take values in $\sigma(x) \in \Sigma = \{0, 1\}$, $\Omega_x = \{x\}$, $\mathcal{S}_x = \{0, 1\}$ and the update represents a spin flip at the site x , i.e., for $z \in \Lambda_N$

$$\sigma^{x,\omega}(z) \equiv \sigma^x(z) = \begin{cases} \sigma(z) & \text{if } z \neq x, \\ 1 - \sigma(x) & \text{if } z = x. \end{cases}$$

2. *Diffusion for single species particles.* The state space for spins is $\sigma(x) \in \Sigma = \{0, 1\}$, $\Omega_x = \{y \in \Lambda_N \mid |x - y| = 1\}$ includes all nearest neighbors of the site x to which a particle can move. Thus the new configuration $\sigma^{x,\omega} = \sigma^{(x,y)}$ is obtained by updating the configuration $S_t = \sigma$ from the set of possible local configuration changes $\{0, 1\}^{\Omega_x}$ using the specific rule, also known as spin exchange, which involves changes at two sites x and $y \in \Omega_x$

$$\sigma^{x,\omega}(z) \equiv \sigma^{(x,y)}(z) = \begin{cases} \sigma(z) & \text{if } z \neq x, y, \\ \sigma(x) & \text{if } z = y, \\ \sigma(y) & \text{if } z = x. \end{cases}$$

The transition rate is then written as $c(x, \omega; \sigma) = c(x, y; \sigma)$. The resulting process $\{S_t\}_{t \geq 0}$ defines dynamics with the total number of particles ($\sum_{x \in \Lambda_N} \sigma(x)$) conserved, sometimes referred to as Kawasaki dynamics.

3. *Multicomponent reactions.* Reactions that involves K species of particles are easily described by enlarging the spin space to $\Sigma = \{0, 1, \dots, K\}$. If the reactions occur only at a single site x , the local configuration space $\mathcal{S}_x = \Sigma$ and the update is indexed by $k \in \Sigma$ with the rule

$$\sigma^{x,\omega}(z) \equiv \sigma^{(x,k)}(z) = \begin{cases} \sigma(z) & \text{if } z \neq x, y, \\ k & \text{if } z = x. \end{cases}$$

The rates $c(x, \omega; \sigma) \equiv c(x, k; \sigma)$ define probability of a transition $\sigma(x)$ to species $k = 1, \dots, K$ or vacating a site, i.e., $k = 0$, over δt .

4. *Reactions involving particles with internal degrees of freedom.* Typically a reaction involves particles with internal degrees of freedom, and in this case several neighboring lattice sites may be updated at the same time, corresponding to the degrees of freedom of the particles involved in the reaction. For example, in a case such as CO oxidation on a catalytic surface, [21], when only particles at a nearest-neighbor distance can react we set $\sigma(x) \in \Sigma = \{0, 1, \dots, K\}$, $\Omega_x = \{y \in \Lambda_N \mid |x - y| = 1\}$ and the set

of local updates $\mathcal{S}_x = \Sigma^{\Omega_x}$. Such \mathcal{S}_x contains all possible reactions in a neighborhood of x . When reactions involve only pairs of species, the rates can be indexed by $k, l \in \Sigma$, or equivalently $\mathcal{S}_x = \Sigma \times \Sigma$. Then the reaction rate $c(x, \omega; \sigma) = c(x, y, k, l; \sigma)$ describes the probability per unit time of $\sigma(x) \rightarrow k$ at the site x and $\sigma(y) \rightarrow l$ at y , i.e., the updating mechanism

$$\sigma^{x, \omega}(z) \equiv \sigma^{(x, y, k, l)}(z) = \begin{cases} \sigma(z) & \text{if } z \neq x, y, \\ k & \text{if } z = x, \\ l & \text{if } z = y, \end{cases}$$

where $|x - y| = 1$.

2.1. Hierarchical structure of the generator

The generator of the Markov process $\{S_t\}_{t \geq 0}$ given in a general form in (3) is our starting point for the development of parallel algorithms based on geometric partitioning of the lattice. The lattice Λ_N is decomposed into non-overlapping cells C_m , $m = 1, \dots, M$ such that

$$\Lambda_N = \bigcup_{m=1}^M C_m, \quad C_m \cap C_n = \emptyset, \quad m \neq n. \quad (5)$$

With each set C_m a larger set \bar{C}_m is associated by adding sites to C_m which are connected with sites in C_m by interactions or the updating mechanism, see Figure 1(a). More precisely, we define the range of interactions L for the set C_m and the closure of this set

$$\bar{C}_m = \{z \in \Lambda_N \mid |z - x| \leq L, x \in C_m\}, \quad \text{where } L = \max_{x \in C_m} \{\text{diam } \Omega_x\}.$$

In many models the value of L is independent of x due to translational invariance of the model. The boundary of C_m is then defined as $\partial C_m = \bar{C}_m \cap C_m$. This geometric partitioning induces a decomposition of the generator (3)

$$\mathcal{L}f(\sigma) = \sum_{x \in \Lambda_N} \sum_{\omega \in \mathcal{S}_x} c(x, \omega; \sigma) [f(\sigma^{x, \omega}) - f(\sigma)] \quad (6)$$

$$= \sum_{m=1}^M \sum_{x \in C_m} \sum_{\omega \in \mathcal{S}_x} c(x, \omega; \sigma) [f(\sigma^{x, \omega}) - f(\sigma)] \quad (7)$$

$$= \sum_{m=1}^M \mathcal{L}_m f(\sigma). \quad (8)$$

The generators \mathcal{L}_m define new Markov processes $\{S_t^m\}_{t \geq 0}$ on the *entire* lattice Λ_N .

Remark: In many models the interactions between particles are of the two-body type with the nearest-neighbor range and therefore the transition rates

$c(x, \omega; \sigma)$ depend on the configuration σ only through $\sigma(x)$ and $\sigma(y)$ with $|x - y| = 1$. Similarly the new configuration $\sigma^{x, \omega}$ involve changes only at the sites in this neighborhood. Thus the generator \mathcal{L}_m updates the lattice sites at most in the set $\bar{C}_m = \{z \mid |x - z| = 1, x \in C_m\}$, see Figure 1(a). Consequently the processes $\{S_t^m\}_{t \geq 0}$ and $\{S_t^{m'}\}_{t \geq 0}$ corresponding to \mathcal{L}_m and $\mathcal{L}_{m'}$ are independent provided $\bar{C}_m \cap \bar{C}_{m'} = \emptyset$.

Therefore, splitting (6) allows us to define independent processes which yields an algorithm suitable for parallel implementation, in particular, in the case of short-range interactions when the communication overhead can be handled efficiently. If the lattice Λ_N is partitioned into subsets C_m such that the diameter $\text{diam} C_m > L$, where L is the range of interactions, we can group the sets $\{C_m\}_{m=1}^M$ in such a way that there is no interaction between sites in the sets C_m that belong to the same group. For the sake of simplicity we assume that the lattice is divided into two *sub-lattices* described by the index sets \mathcal{I}^E and \mathcal{I}^O , (black vs. white in Fig. 1(a)), hence we have

$$\Lambda_N = \Lambda_N^E \cup \Lambda_N^O := \bigcup_{m \in \mathcal{I}^E} C_m^E \cup \bigcup_{m \in \mathcal{I}^O} C_m^O. \quad (9)$$

Other lattice partitionings are also possible and may be more suitable for specific micro-mechanisms in the KMC or the computer architecture. Choice of the partitioning scheme can reduce communication overhead, see for instance [34]. For the sake of simplicity in the presentation, here we consider the partitioning depicted in (9) and Fig. 1(a), although our mathematical framework applies to any other sublattice decomposition. Returning to (9), the sub-lattices *induce* a corresponding splitting of the generator:

$$\mathcal{L} = \mathcal{L}^E + \mathcal{L}^O := \sum_{m \in \mathcal{I}^E} \mathcal{L}_m^E + \sum_{m \in \mathcal{I}^O} \mathcal{L}_m^O. \quad (10)$$

This simple observation has key consequences for simulating the process $\{S_t\}_{t \geq 0}$ in parallel, as well as formulating different related algorithms: the processes $\{S_t^m\}_{t \geq 0}$ corresponding to the generators \mathcal{L}_m^E are mutually independent for different $m \in \mathcal{I}^E$, and thus can be simulated in parallel; similarly we can handle the processes belonging to the group indexed by \mathcal{I}^O . However, there is still communication between these two groups as there is non-empty overlap between the groups due to interactions and updates in the sets $\partial C_m, \partial C_{m'}$ when $m \in \mathcal{I}^E$ and $m' \in \mathcal{I}^O$ and the cells are within the interaction range L . To handle this communication we next introduce a Fractional Step approximation of the Markov semigroup $e^{t\mathcal{L}}$ associated with the process $\{S_t\}_{t \geq 0}$.

2.2. Fractional Step Kinetic Monte Carlo Algorithms

The deterministic Trotter Theorem was first proved in [36] for the approximation of semigroups corresponding to operator sums, and it has found wide application in the numerical ODE/PDE analysis, e.g., [12]. Similarly, the key

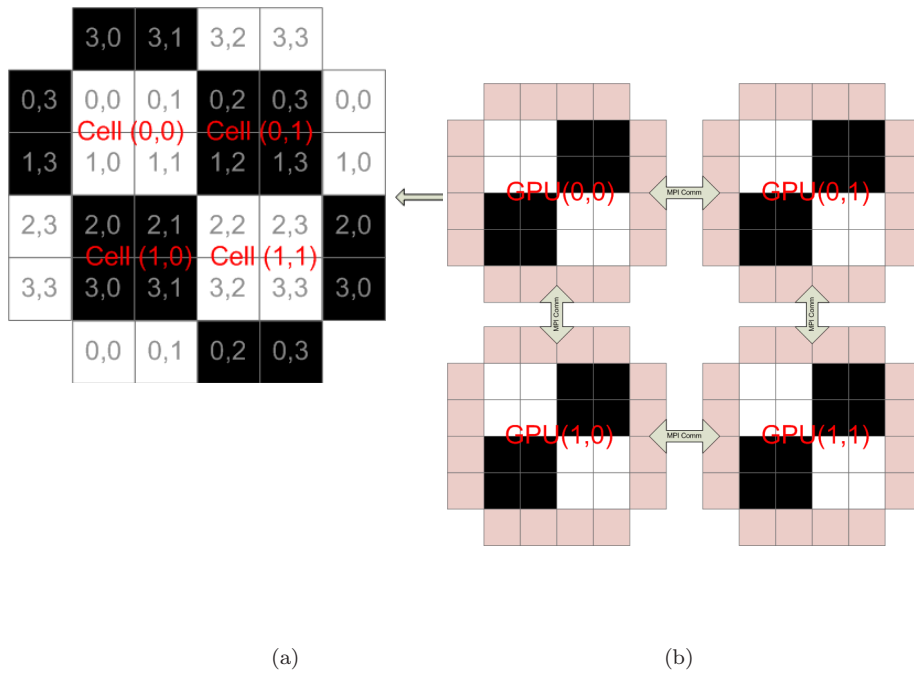


Figure 1: (a) Lattice decomposition in (9) using the checkerboard scheme mapped onto a single multi-threading processing unit (e.g., GPU). The integer cell coordinates also indicate communication through boundary buffer regions. In practice other partitionings may result in a lower communication overhead. (b) Hierarchical lattice partitioning on a cluster of processing units.

tool for our analysis is a deterministic as well as a stochastic version of the Trotter formula, [18], applied to the operator $\mathcal{L} = \mathcal{L}^E + \mathcal{L}^O$

$$e^{t\mathcal{L}} = \lim_{n \rightarrow \infty} \left[e^{\frac{t}{n}\mathcal{L}^E} e^{\frac{t}{n}\mathcal{L}^O} \right]^n. \quad (11)$$

The proposed parallel scheme uses the fact that the action of the operator \mathcal{L}^E (and similarly of \mathcal{L}^O) can be distributed onto independent processing units. Thus to reach a time T we define a time step $\Delta t = \frac{T}{n}$ for a fixed value of n and alternate the evolution by \mathcal{L}^E and \mathcal{L}^O . More precisely, (11) gives rise to the *Lie* splitting approximation for $n \gg 1$:

$$e^{T\mathcal{L}} \approx \left[e^{\frac{T}{n}\mathcal{L}^E} e^{\frac{T}{n}\mathcal{L}^O} \right]^n. \quad (12)$$

Since the simulated systems exhibit short-range interactions, the generators $\mathcal{L}_k^E, \mathcal{L}_l^E$ commute for $k, l \in \mathcal{I}^E$, $k \neq l$:

$$\mathcal{L}_k^E \mathcal{L}_l^E - \mathcal{L}_l^E \mathcal{L}_k^E = 0, \quad \text{for all } k, l \in \mathcal{I}^E, k \neq l.$$

Hence, [36], we have the exact formula

$$e^{\Delta t \mathcal{L}^E} e^{\Delta t \mathcal{L}^O} = \prod_{m \in \mathcal{I}^E} e^{\Delta t \mathcal{L}_m^E} \prod_{m \in \mathcal{I}^O} e^{\Delta t \mathcal{L}_m^O}. \quad (13)$$

Then the expression (13) implies that the KMC solvers corresponding to the semigroup $e^{\Delta t \mathcal{L}^E}$ (resp. $e^{\Delta t \mathcal{L}^O}$) can be simulated *exactly* by breaking down the task into separate processors/threads for each $m \in \mathcal{I}^E$ (resp. $m \in \mathcal{I}^O$). Therefore, this scheme allows us to run independently on each fractional time-step window Δt , and on every processor, a serial KMC simulation, called a *kernel*. The resulting computational framework consisting of the hierarchical decomposition (10) and (12) permits to input as the algorithm's kernel any preferred optimized serial KMC algorithm.

A single time step of the parallel algorithm is thus easily described in the following stages:

Step 1–Evolution by \mathcal{L}^E : Simulate independent Markov processes $\{S_t^m\}_{t \geq 0}$, $m \in \mathcal{I}^E$ by a kinetic Monte Carlo kernel running on non-communicating processors that correspond to each C_m for time Δt .

Step 2–Local Synchronization: communicate configurations σ^E from overlapping domains $\bar{C}_m^E \cap \bar{C}_n^O$ in order to update configurations σ^O .

Step 3–Evolution by \mathcal{L}^O : Simulate independent Markov processes $\{S_t^m\}_{t \geq 0}$, $m \in \mathcal{I}^O$ by a KMC *kernel* on non-communicating processors that correspond to each C_m for time Δt .

We emphasize that the resulting process $\{\tilde{S}_t\}_{t \geq 0}$ is an *approximation* of the process $\{S_t\}_{t \geq 0}$ and we discuss its features and properties in the next two sections.

3. Processor Communication Schedule and Random Trotter Products

A key feature of the fractional step methods is the *Processor Communication Schedule* (PCS) that dictates the order with which the hierarchy of operators in (6) are applied and for how long. For instance, in (12) the processors corresponding to \mathcal{L}^E (resp. \mathcal{L}^O) do not communicate, hence the processor communication within the algorithm occurs *only* each time we have to apply $e^{\frac{T}{2n}\mathcal{L}^E}$ or $e^{\frac{T}{2n}\mathcal{L}^O}$. Therefore we can define as the PCS the (deterministic) jump process $X = X(t)$, $t \in [0, T]$, where $[0, T]$ is the simulated time window and taking values in the set $\mathcal{X} = \{1, 2\}$, where we assign the value 1 (resp. 2) to O (resp. E):

$$X(t) = 1, \quad \frac{2kT}{n} \leq t < \frac{(2k+1)T}{n}, \quad (14)$$

$$X(t) = 2, \quad \frac{(2k+1)T}{n} \leq t < \frac{(2k+2)T}{n}. \quad (15)$$

for all $k = 0, \dots, n-1$. Processor communication occurs at jump times, while in the remaining time the processors operate independently and do not communicate. In an analogous way we can define the PCS for the *Strang* splitting scheme (16),

$$e^{T\mathcal{L}} \approx \left[e^{\frac{T}{2n}\mathcal{L}^E} e^{\frac{T}{n}\mathcal{L}^O} e^{\frac{T}{2n}\mathcal{L}^E} \right]^n, \quad (16)$$

with the scheduling process

$$X(t) = 1, \quad \frac{2kT}{2n} \leq t < \frac{(2k+1)T}{2n}, \quad (17)$$

$$X(t) = 2, \quad \frac{(2k+1)T}{2n} \leq t < \frac{(2k+3)T}{2n}, \quad (18)$$

$$X(t) = 1, \quad \frac{(2k+3)T}{2n} \leq t < \frac{(2k+4)T}{2n}, \quad (19)$$

for all $k = 0, \dots, n-1$.

3.1. Random Fractional Step Methods

In both cases above (12) and (16), the communication schedule is fully deterministic, relying on the Trotter Theorem (11). On the other hand, we can construct stochastic PCS based on the *Random Trotter Product* Theorem, and as we show below the sub-lattice algorithm proposed in [34] is a fractional step algorithm with stochastic PCS.

The Random Trotter Product Theorem, [18], extends (11) as follows: We consider a sequence of semigroups $e^{T\mathcal{L}^\xi}$ with corresponding operators \mathcal{L}_ξ where ξ is in the index set \mathcal{X} , assuming for simplicity \mathcal{X} is finite, although a much more general setting is possible, (25). Consider also a stochastic jump process $X = X(t)$ with \mathcal{X} as its state space. For each of its trajectories we denote by $\xi_0, \xi_1, \dots, \xi_n$ the (typically random) sequence of states visited by the stochastic

process $X(t)$ and $\tau_0, \tau_1, \dots, \tau_n$ the corresponding (also typically random) jump times

$$X(t) = \xi_0, \quad 0 \leq t < \tau_0, \quad (20)$$

$$X(t) = \xi_1, \quad \tau_0 \leq t < \tau_1, \quad (21)$$

$$\dots \quad (22)$$

$$X(t) = \xi_k, \quad \tau_{k-1} \leq t < \tau_k. \quad (23)$$

We additionally define as $N(t)$ the number of jumps up to time t . We assume that $X(t)$ is selected so that it has an ergodic behavior, i.e., there is a probability measure $\mu(d\xi)$ such that for all bounded functions g we have that

$$\lim_{t \rightarrow \infty} \frac{1}{t} \int_0^t g(X(s)) ds = \int g(\xi) \mu(d\xi). \quad (24)$$

For example, if $X(t)$ is a Markov process then under suitable conditions, (24) will hold, where μ will be the stationary distribution of $X(t)$, [20]. Conversely, it is well-known that for a given μ we can construct in a non-unique way Markov processes $X(t)$ which satisfy the condition (24), [20]. Now we can state the Random Trotter Product Theorem, [18], in analogy to (11):

$$e^{T\bar{\mathcal{L}}} = \lim_{n \rightarrow \infty} \left[e^{\frac{\tau_0}{n} \mathcal{L}_{\xi_0}} e^{\frac{\tau_1 - \tau_0}{n} \mathcal{L}_{\xi_1}} \dots e^{\frac{nT - \tau_{N(nt)}}{n} \mathcal{L}_{\xi_{N(nt)}}} \right], \quad (25)$$

where the operator $\bar{\mathcal{L}}$ is defined on any bounded function as

$$\bar{\mathcal{L}}g = \int \mathcal{L}_\xi \mu(d\xi). \quad (26)$$

It is clear that (12) is a special case of (25) when $\tau_k - \tau_{k-1} = 1$ and $\xi_{2k} = 1$, $\xi_{2k+1} = 2$ for all k . Similarly, we can also view (16) as a deterministic analogue of (25).

On the other hand, in the context of the parallel fractional step algorithms for KMC introduced here, the random process (20) can be interpreted as a stochastic PCS. For example, the sub-lattice (SL) parallelization algorithm for KMC, introduced in [34], is a fractional step algorithm with stochastic PCS: indeed, in this method the lattice is divided into sub-lattices, for instance as in (9), $\Lambda_N = \Lambda_N^E \cup \Lambda_N^O$. Each sub-lattice is selected *at random* and advanced by KMC over a fixed time window Δt . Then a new random selection is made and again the sub-lattice is advanced by Δt , and so on. The procedure is parallelizable as cells C_m^E, C_m^O within each sub-lattice do not communicate. This algorithm is easily recast as a fractional step approximation, when in (20) we select deterministic jump times τ_k and random variables ξ_k :

$$\frac{\tau_k - \tau_{k-1}}{n} = \Delta t, \quad \text{and} \quad P(\xi_k = 1) = P(\xi_k = 2) = \frac{1}{2}. \quad (27)$$

As in (14), here we assign the value 1 (resp. 2) to the O (resp. E) sub-lattice. Furthermore, we can easily calculate (26) to obtain

$$\bar{\mathcal{L}}g = \frac{1}{2} (\mathcal{L}^E + \mathcal{L}^O) ,$$

which is just a time rescaling of the original operator \mathcal{L} . Thus the SL algorithm is rewritten as the fractional step approximation with the stochastic PCS (27) as

$$e^{T\bar{\mathcal{L}}} \approx e^{\frac{\tau_0}{n}\mathcal{L}_{\xi_0}} e^{\frac{\tau_1-\tau_0}{n}\mathcal{L}_{\xi_1}} \dots e^{\frac{nT-\tau_N(nt)}{n}\mathcal{L}_{\xi_N(nt)}} . \quad (28)$$

From the numerical analysis viewpoint, our re-interpretation of the SL algorithm in [34] as a fractional step scheme allows us to also provide a mathematically rigorous justification that it is a *consistent* estimator of the serial KMC algorithm, due to the Random Trotter Theorem (25). That is, as the time step in the fractional step scheme converges to zero, it converges to the continuous time Markov Chain that has the same master equation and generator as the original serial KMC. Finally, the (deterministic) Trotter Theorem (11) also implies that the Lie and the Strang schemes are, in the numerical analysis sense, consistent approximations of the serial KMC algorithm.

4. Controlled Error Approximations of KMC

In this section we present a formal argument for the error analysis of the fractional step approximations for KMC, which suggests the order of convergence of the schemes, as well as the restrictions on the Fractional Step KMC time step Δt . In the decomposition (10) the operators are linear operators on the high, but finite-dimensional configuration space \mathcal{S} , hence by the standard error analysis of splitting schemes, see [12], we have

$$e^{\Delta t\mathcal{L}} - e^{\Delta t\mathcal{L}^E} e^{\Delta t\mathcal{L}^O} = [\mathcal{L}^E\mathcal{L}^O - \mathcal{L}^O\mathcal{L}^E] \frac{(\Delta t)^2}{2} + \mathcal{O}(\Delta t^3) , \quad (29)$$

where we readily see that the term $[\mathcal{L}^E, \mathcal{L}^O] := \mathcal{L}^E\mathcal{L}^O - \mathcal{L}^O\mathcal{L}^E$ is the Lie bracket (commutator) of the operators $\mathcal{L}^E, \mathcal{L}^O$. This Lie bracket captures the effect of the boundary regions $\bar{C}_m^E \cap \bar{C}_n^O$ through which we have processor communication: if there was no communication the Lie bracket would be exactly zero.

Furthermore, instead of (12) we can consider the *Strang-type* splitting (16). As in the ODE case, [12], this is expected to yield a higher order error term $\mathcal{O}(\Delta t^3)$ instead of the second order approximation in (29), in the following sense:

$$e^{\Delta t\mathcal{L}} - e^{\frac{\Delta t}{2}\mathcal{L}^E} e^{\Delta t\mathcal{L}^O} e^{\frac{\Delta t}{2}\mathcal{L}^E} = \left\{ \frac{1}{12} [\mathcal{L}^O, [\mathcal{L}^O, \mathcal{L}^E]] - \frac{1}{24} [\mathcal{L}^E, [\mathcal{L}^E, \mathcal{L}^O]] \right\} (\Delta t)^3 + \mathcal{O}(\Delta t^4) . \quad (30)$$

Such calculations suggest that the Strang splitting leads to a more accurate scheme, which is balanced by more complicated boundary local communication in the same time window Δt , as is evident when comparing (12) and (16).

Next, we briefly comment on the error estimation suggested by the calculation (29) and return to the rigorous numerical analysis in [1]. In order to obtain an estimate in the right-hand side of (29) which is independent of the system size N , it is essential to obtain an upper bound on the total number of jumps up to the time T . This is a key point related to the *extensivity* of the system and to the fact that the weak error analysis is restricted (as it should be physically) to mesoscopic observables satisfying (44). We observe the dependence of the error on mesoscopic observables in the following subsection. In the context of coarse-graining, in [15] an analogous estimate was shown rigorously using a Bernstein-type argument applied to the discrete derivatives, in the spirit of (44), of the solutions to the backward Kolmogorov equation. We refer to such bounds as “Bernstein-like” due to their similarity to gradient estimates for linear and nonlinear parabolic PDEs.

4.1. Error Analysis and comparison between random and deterministic PCS

In this section we further demonstrate the use of the operator splitting formulation as a numerical analysis tool by comparing the time-step of Δt the random PCS introduced in [34] to the deterministic Lie PCS introduced in (12). A similar comparison can be made for the Strang scheme (16). A detailed discussion including rigorous error estimates for mesoscopic observables such as (44), which are independent of the lattice size N will be discussed in [1].

Here we focus on the example of adsorption/desorption discussed in Section 2. The generator in the one space dimension is decomposed as in (10)

$$\mathcal{L}^E f(\sigma) = \sum_{x \in \Lambda} c^E(x, \sigma) \left(f(\sigma^x) - f(\sigma) \right),$$

and

$$\mathcal{L}^O f(\sigma) = \sum_{x \in \Lambda} c^O(x, \sigma) \left(f(\sigma^x) - f(\sigma) \right),$$

where

$$c^E(x, \sigma) = \begin{cases} c(x, \sigma), & x \in \Lambda_N^E \\ 0, & \text{otherwise} \end{cases} \quad c^O(x, \sigma) = \begin{cases} c(x, \sigma), & x \in \Lambda_N^O \\ 0, & \text{otherwise} \end{cases}$$

and the sub-lattices Λ_N^E, Λ_N^O are defined in (9). The rates $c(x, \sigma)$ of the corresponding generator (3) for the case of Arrhenius adsorption/desorption are given by

$$c(x, \sigma) = c_a(1 - \sigma(x)) + c_d \sigma(x) \exp(-\beta U(x, \sigma)), \quad (31)$$

where c_a and c_d are the adsorption and desorption constants respectively, [7]. The desorption potential $U = U(x, \sigma)$ is defined as

$$U(x, \sigma) = \sum_{y \neq x} J(x - y) \sigma(y), \quad (32)$$

where $J = J(x - y)$ is the lateral interaction potential; for simplicity we assume that the range of interactions is L , while in typical simplified nearest neighbor

models $L = 1$. Similarly we define diffusion dynamics with Arrhenius dynamics, [14].

First we discuss the error analysis for the Lie splitting scheme. For given finite lattice size N , in the decomposition (10) the operators are linear operators on the high, but finite-dimensional configuration space \mathcal{S} , hence by the standard error analysis of Lie splitting schemes, we obtain (29). A more careful study of the commutator reveals that the generator decomposition (10) induces significant cancellations in the evaluation of the generator: indeed, we define

$$C_m^o = C_m \setminus \partial C_m, \quad C_m = C_m^o \cup C_m^\partial,$$

where in Section 2 we introduced $\partial C_m = \bar{C}_m \cap C_m$ and $\bar{C}_m = \{z \in \Lambda_N \mid |z - x| \leq L, x \in C_m\}$. Thus, in (10) we obtain the further decomposition

$$\mathcal{L}^E = \mathcal{L}^{E,o} + \mathcal{L}^{E,\partial} := \sum_{m \in \mathcal{I}^E} \mathcal{L}_m^{E,o} + \mathcal{L}_m^{E,\partial}, \quad (33)$$

where $\mathcal{L}_m^{E,o}, \mathcal{L}_m^{E,\partial}$ is the restriction of \mathcal{L}^E on C_m^o and C_m^∂ respectively. Analogously we define $\mathcal{L}^O = \mathcal{L}^{O,o} + \mathcal{L}^{O,\partial}$. We now return to the evaluation of the commutator

$$[\mathcal{L}^E, \mathcal{L}^O] = [\mathcal{L}^{E,\partial}, \mathcal{L}^{O,\partial}] + [\mathcal{L}^{E,o}, \mathcal{L}^{O,o}] + [\mathcal{L}^{E,\partial}, \mathcal{L}^{O,o}] + [\mathcal{L}^{E,o}, \mathcal{L}^{O,\partial}]. \quad (34)$$

However, due to the lack of communication between generators beyond the interaction range, we have that

$$[\mathcal{L}^{E,o}, \mathcal{L}^{O,o}] = 0, \quad [\mathcal{L}^{E,\partial}, \mathcal{L}^{O,o}] = 0, \quad [\mathcal{L}^{E,o}, \mathcal{L}^{O,\partial}] = 0,$$

thus we readily get

$$[\mathcal{L}^E, \mathcal{L}^O] = [\mathcal{L}^{E,\partial}, \mathcal{L}^{O,\partial}] = \sum_{m \in \mathcal{I}^E} \sum_{\substack{l \in \mathcal{I}^O \\ |l-m|=1}} [\mathcal{L}_m^{E,\partial}, \mathcal{L}_l^{O,\partial}]. \quad (35)$$

The formula (35) captures the processor communication between boundary regions of \bar{C}_m^E, \bar{C}_n^O . But more importantly, when combined with (29), it suggests the limitations on the time window Δt of the Lie scheme (12), denoted for differentiation by Δt_{Lie} , in order to obtain a given error tolerance TOL. In that sense it is useful to obtain an upper bound on (35). Indeed, we readily obtain:

$$\begin{aligned} [\mathcal{L}^E, \mathcal{L}^O]f(\sigma) &= \sum_{\substack{m \in \mathcal{I}^E, l \in \mathcal{I}^O \\ |l-m|=1}} \sum_{x,y} \left[c^E(x, \sigma) c^O(y, \sigma^x) - c^E(x, \sigma^y) c^O(y, \sigma) \right] f((\sigma^x)^y) \\ &\quad - \sum_{x,y} c^E(x, \sigma) \left[c^O(y, \sigma^x) - c^O(y, \sigma) \right] f(\sigma^x) \\ &\quad - \sum_{x,y} c^O(y, \sigma) \left[c^E(x, \sigma) - c^E(x, \sigma^y) \right] f(\sigma^y) \end{aligned} \quad (36)$$

where all summations are over $x \in C_m^{E,\partial}, y \in C_l^{O,\partial}$. For *mesoscopic observables*, such as the mean coverage $f(\sigma) = \frac{1}{N} \sum_{x \in \Lambda} \sigma(x)$ we obtain

$$\begin{aligned} [\mathcal{L}^E, \mathcal{L}^O]f(\sigma) = & \sum_{\substack{m \in \mathcal{I}^E, l \in \mathcal{I}^O \\ |l-m|=1}} \sum_{x,y} c^O(y, \sigma) \left[c^E(x, \sigma) - c^E(x, \sigma^y) \right] \frac{1 - 2\sigma(x)}{N} \\ & + \sum_{x,y} c^E(x, \sigma) \left[c^O(y, \sigma^x) - c^O(y, \sigma) \right] \frac{1 - 2\sigma(y)}{N}, \end{aligned} \quad (37)$$

where all summations are over $x \in C_m^{E,\partial}, y \in C_l^{O,\partial}$. Therefore, due to the *cancellation* of all interior components $\mathcal{L}^{E,o}, \mathcal{L}^{O,o}$ in (35), we obtain the bound for the case of the interaction range $L = 1$,

$$|[\mathcal{L}^E, \mathcal{L}^O]f(\sigma)| \sim O\left(\frac{M \cdot L}{N}\right) = O\left(\frac{1}{q}\right), \quad (38)$$

where q is the size of each cell C_m , and $O(1)$ depends on the physical parameters in the rate (31). The local error analysis in (29), (38) can be propagated up to a prescribed time $T = N_{\text{Lie}} \Delta t_{\text{Lie}}$. Therefore, for the simulation of the mesoscopic observable f up to the time T within a given error tolerance TOL, (29) and (38) give the *observable-dependent* relation for the Lie time step

$$\text{TOL} \sim T \cdot |[\mathcal{L}^E, \mathcal{L}^O]f(\sigma)| \Delta t_{\text{Lie}} \sim T \cdot O\left(\frac{1}{q}\right) \Delta t_{\text{Lie}} \quad (39)$$

Next, using the fractional step formulation, we analyze in the same spirit as for the Lie scheme, the random PCS (27) proposed in [34]. For notational simplicity we set $A_1 = \mathcal{L}^O$, $A_2 = \mathcal{L}^E$. Then the local error operator $E^{\Delta t}$ can also be calculated as in (29):

$$\begin{aligned} \text{Local Error} = E^{\Delta t} & := e^{\Delta t A_{\xi_1}} e^{\Delta t A_{\xi_2}} - e^{\Delta t (A_1 + A_2)} \\ & = \left(I + (A_{\xi_1} + A_{\xi_2}) \Delta t + \frac{1}{2} (A_{\xi_1}^2 + 2A_{\xi_1} A_{\xi_2} + A_{\xi_2}^2) \Delta t^2 \right) - \\ & \quad \left(I + (A_1 + A_2) \Delta t + \frac{1}{2} (A_1 + A_2)^2 \Delta t^2 \right) + O(\Delta t^3) \end{aligned} \quad (40)$$

The mean value of the error over the sequence of independent random variables $\xi = (\xi_i, i = 1, \dots, n)$ of the PCS (27) on an observable $f = f(\sigma), s \in \mathcal{S}$ can be explicitly evaluated:

$$\mathbb{E}_\xi [E^{\Delta t} f] = \frac{1}{4} (A_1 - A_2)^2 f \Delta t^2 + O(\Delta t^3) = \frac{1}{4} (\mathcal{L}^E - \mathcal{L}^O)^2 f \Delta t^2 + O(\Delta t^3).$$

As in (38), for the mesoscopic observable $f(\sigma) = \frac{1}{N} \sum_{x \in \Lambda} \sigma(x)$, we obtain, after disregarding the higher order local error $O(\Delta t^3)$,

$$(\mathcal{L}^E - \mathcal{L}^O)^2 f(\sigma) \sim O(1), \quad (41)$$

where $O(1)$ depends on the physical parameters in the rate (31). Similarly to (39), for the simulation of the mesoscopic observable f up to the same prescribed time $T = N_{\text{Random}} \Delta t_{\text{Random}}$, within the same error tolerance TOL, (29) and (41) give the *observable*-dependent relation for the random PCS time step

$$\text{TOL} \sim T \cdot |(\mathcal{L}^E - \mathcal{L}^O)^2 f(\sigma)| \Delta t_{\text{Random}} \sim T \cdot O(1) \Delta t_{\text{Random}} \quad (42)$$

Comparing the random and the Lie PCS through (39) and (42) implies that in order the two schemes to conform (in the mean) to the same tolerance TOL, their respective time steps should be selected so that

$$\Delta t_{\text{Lie}} \sim O(q) \Delta t_{\text{Random}} \quad (43)$$

This relation in turn suggests that the Lie scheme (12) is expected to parallelize better than the random PCS (27) since it allows a q -times larger time step Δt for the same accuracy, keeping in mind that during each time step processors do not communicate.

A similar analysis is possible for general mesoscopic observables $f = f(\sigma)$, $s \in \mathcal{S}$, e.g., spatial correlations, that satisfy

$$\sum_{x \in \Lambda_N} |f(\sigma^x) - f(\sigma)| \leq C \quad (44)$$

where C is a constant independent of N , see the formulation and estimates for coarse-grained stochastic systems in [15]. We revisit this issue, as well as the rigorous derivation of N -independent error bounds in place of the expansions (29), (30) in the upcoming publication [1]. Such estimates can also allow a detailed analysis on the balance between accuracy and local processor communication for PCS such as (12), (16) and (27).

5. Hierarchical structure of Fractional Step algorithms and implementation on GPUs

The fractional step framework allows a hierarchical structure to be easily formulated and implemented, which is a key advantage for simulating in parallel architectures with complex memory hierarchies and processing units. The Graphical Processing Unit (GPU) architecture is inherently different from a traditional CPU architecture. GPUs are massively parallel multi-threaded devices capable of executing a large number of active threads concurrently. A GPU consists of multiple streaming multiprocessors (MP), each of which contains multiple scalar processor cores. For example, NVIDIA's C2050 GPU architecture contains 14 such multiprocessors, each of which contains 32 cores, for a total of 448 cores which can handle up to 24k active threads in parallel. A GPU has several types of memory which are differently organized compared to the traditional hierarchical CPU memory, most notably the main device memory (global memory) shared between all the multiprocessors and the on-chip memory shared between all cores of a single multiprocessor (shared memory). The

memory sizes and access speeds depend on the type of GPU. For instance, the memory size of the NVIDIA C2050 GPU is 3GB while the memory size of the NVIDIA C2070 GPU is 6GB.

From the perspective of a GPU programmer writing a code for NVIDIA GPU's, the GPU is treated as a co-processor to the main CPU. Programs are written in C and linked to the CUDA libraries. A function that executes on the GPU, called a GPU kernel, consists of multiple threads executing code in a single instruction, multiple data (SIMD) fashion. That is, each thread in a GPU kernel executes the same code, but on different data. Further, threads can be grouped into thread blocks. This abstraction takes advantage of the fact that threads executing on the same multiprocessor can share data via on-chip shared memory, allowing some degree of cooperation between threads in the same block [32]. A major drawback in GPU programming is the slow communication between GPU global memory and the main memory of the CPU, compared to the communication within a GPU. Programmers address this problem by maximizing the amount of arithmetic intensive computations performed on GPU, minimizing the communication between CPU and GPU, and allowing the communication latency to be hidden by overlapping with execution. Communication among GPUs, although costly, is enabled by APIs such as OpenMP and features available in CUDA 2.2+ such as portable pinned memory, when the communication is among GPUs connected to the same shared-memory computer node. When the communication takes place among GPUs across nodes of a cluster, message passing paradigms such as MPI can serve the same scope.

In our parallelization of the KMC method, we redefine the data structures to represent lattice sites in the simulation so that the whole simulated system is cut into equal-sized black and white coarse cells like a chessboard in (9). For instance, Fig. 1(a) shows a simple example in which we map a 4×4 lattice sites into 2×2 cells, each cell containing 2×2 sites. One GPU thread is assigned to one cell. Coverage information of the whole lattice is stored in an array located in the GPU global memory so that all the threads can access the information related to their neighboring sites across MPs. The GPU kernel performing the KMC simulation over the whole lattice by using the Lie scheme (12) and the decomposition (10), is sequentially launched twice for each synchronization time step Δt to work on the black and white cells respectively. The execution times for lattices of different sizes are compared in Fig 2, where we take as a reference a sequential KMC-kernel, which is a direct numerical implementation of (1) and (2). The same kernel is then used for the implementation on GPUs where we compare times for different choices of Δt . We remark that the KMC kernel is not optimized by techniques such as the BKL algorithm, [6, 19], which is also manifested in the scaling with respect to the size of the lattice N . However, the same kernel is used in the Fractional Step algorithm thus here we present comparisons between the same KMC algorithms, one serial and one parallelized by the Fractional Step approach. Clearly any optimized KMC kernel can be used without difficulty in our framework.

The size of lattices that can be simulated on a single GPU is limited by memory, thus in order to simulate large systems it will be necessary to employ a

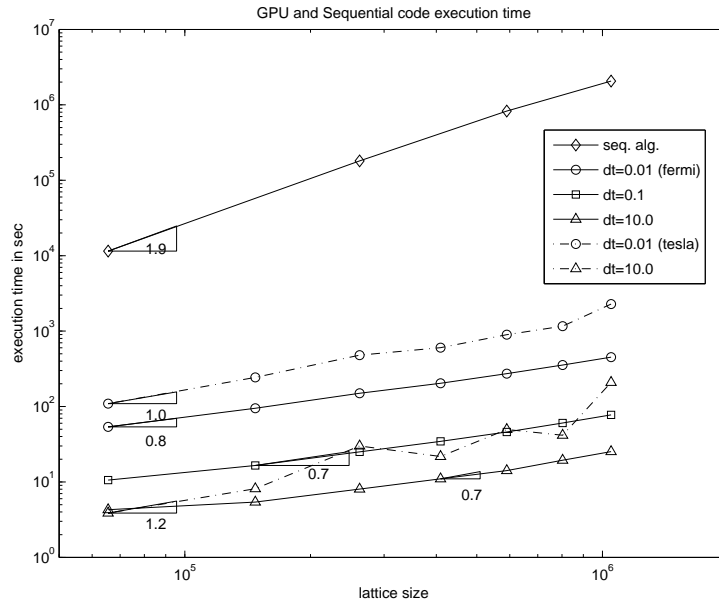


Figure 2: Execution time of the fractional step KMC for lattices of different sizes. The comparison with the sequential algorithm (top curve) is based on the same SSA KMC implementation which, however, does not have the optimal complexity of the BKL algorithm. The simpler implementation of the SSA algorithm was used. The simple implementation has the complexity $\mathcal{O}(N^2)$, where N is the total number of lattice sites. This complexity is reflected in the indicated scaling (the slope in the log-log plot). Note that the due to partitioning of the lattice in the fractional step algorithm the same KMC kernel will scale as $\mathcal{O}(N)$ only, which is in agreement with the observed slope in the plots.

cluster of GPUs communicating, for instance, through an MPI protocol. We will demonstrate next how Fractional Step KMC algorithms can be tailored to an architecture that involves multiple GPUs. We return to the formulation in (10), and consider the sub-lattice decomposition (9). In this formulation each one of the coarse-cells C_m^E or C_m^O are simulated on a single GPU. Within each one of the GPUs we have the same lattice decomposition as in (9), see Figure 1(b), namely

$$C_m^E = C_m^{EE} \cup C_m^{EO} := \bigcup_{l=1}^L D_{ml}^{EE} \cup \bigcup_{l=1}^L D_{ml}^{EO}, \quad (45)$$

and similarly we define a decomposition for C_m^O . Each one of the (sub-)sub-lattices D_{ml}^{EE} and D_{ml}^{EO} corresponds to individual threads within the GPU. Next, (9) and (45) define *nested sub-lattices*, which yield a hierarchical decomposition of the operator \mathcal{L} into (10) and

$$\mathcal{L}_m^E = \mathcal{L}_m^{EE} + \mathcal{L}_m^{EO} := \sum_{l=1}^L \mathcal{L}_{ml}^{EE} + \sum_{l=1}^L \mathcal{L}_{ml}^{EO}, \quad (46)$$

and similarly we also define the decomposition for \mathcal{L}_m^O . Finally, schemes such as (12) and (16) give rise to Fractional Step algorithms based on the nested decompositions (10) and (46). In this case, boundary communication, see Fig. 1(b), plays a key role in the parallelization of our algorithm when multiple GPUs are required. As we discussed earlier, this scenario happens when the lattice size grows to the point that the lattice data structures no longer fit into a single GPU global memory. In turn, this threshold depends on the type of GPU used, e.g., for a NVIDIA's C2050 GPU the maximum lattice size is currently $8,182 \times 8,182$ cells. To simulate larger systems, we can decompose the domain into regular sub-domains and distribute both the sub-domain cells and associated computation among multiple GPUs, as discussed in (46). Boundary communication between two adjacent sub-domains are exchanged between GPUs, see Fig. 1(b), and supported by either MPI or OpenMP, depending on the fact that the GPUs are located on the same cluster node or across nodes. Thus, the multi-GPU parallel KMC algorithm is based on and benefits from the hierarchical structure of the Fractional Step KMC algorithms discussed in (46). At the same time, it can enable the scalability of our simulations to lattice sizes beyond the ones accessible with a single GPU e.g., $8,182 \times 8,182$ sites in a C2050 GPU. The study of performance and scalability of our multi-GPU algorithm and code for different lattice sizes and types of GPU clusters is beyond the scope of this paper.

6. Mass Transport and Dynamic Workload Balancing

Due to the spatially distributed nature of KMC simulations and the dependence of jump rates on local coverage, (1), fractional step algorithms may have an imbalance in the number of operations/jumps performed in each coarse cell C_m in (9), as well as on the corresponding processors. In fact, formulas (1) and

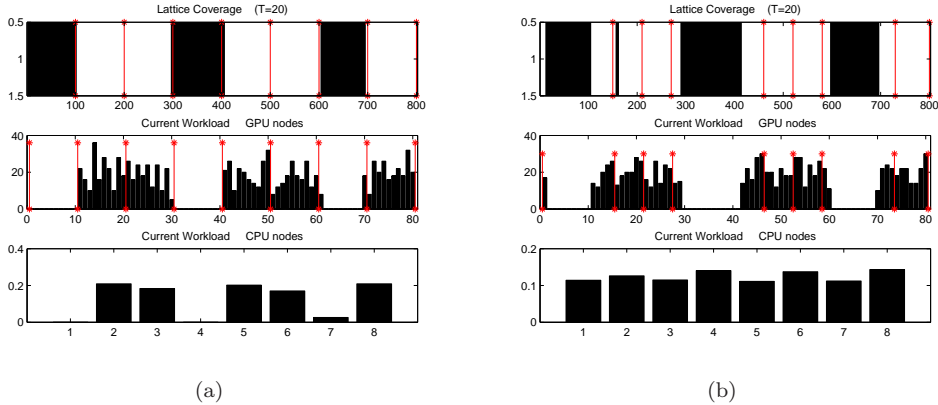


Figure 3: (a) Workload imbalance in 1D unimolecular reaction system: the top figure depicts local coverage, the bottom figure workload distribution; (b) Workload redistribution in Figure (a) using the mass transport for re-balancing.

(2), and the very structure of the fractional step algorithms (10), allow us to define the *workload* $W_{n\Delta t}(\sigma) = W_{n\Delta t}(m; \sigma)$, $1 \leq m \leq M$ as

$$W_{n\Delta t}(m) = \# \text{ jumps in } C_m \text{ during } [(n-1)\Delta t, n\Delta t], \quad (47)$$

when the configuration at time $(n-1)\Delta t$ is σ . We also renormalize $W_{n\Delta t}$ (and still denote it with the same symbol) in order to obtain a histogram, i.e., a probability density. Since different coarse cells C_m in the fractional step algorithms such as (12) or (16) do not communicate during intervals of length Δt the quantities (47) are easy to keep track on-the-fly during the simulations. The possibility of workload imbalance is depicted in Figure 3, where many more jumps are performed in the processors corresponding to cells of low coverage, while the other processors remain idle.

In this Section we introduce a probabilistic strategy to re-balance the workload $W_{n\Delta t}$ dynamically during the simulation based on the following idea from *Mass Transport* methods, e.g., [10]. One wants to transport the “imbalanced” density $W_{n\Delta t}$ into an almost uniform density over the number of processors used, in order to ensure that they remain as uniformly active as possible. The mass transport connection and terminology refers to the mapping of a given probability measure into a desirable probability measure. Typically, [10], this problem is posed as an optimization over a suitable cost functional and is known as the Monge-Kantorovich problem. In our context the cost functional could reflect constraints related to various parallel architectures.

We can formulate and implement this strategy in several different ways: probably the simplest approach, that serves mostly as an illustration, is to assume that we have a number of processors P , where $P \ll M$; during the interval $[(n-1)\Delta t, n\Delta t]$ a number of coarse cells C_m , $1 \leq m \leq M$, which are simulated independently in a fractional step algorithm, are allocated to

each processor. By the end of the simulation time $n\Delta t$ the workload on all processors is described similarly to (47), by a histogram $R_{n\Delta t}(\sigma) = R_{n\Delta t}(l; \sigma)$, $1 \leq l \leq P$. One wants to map (47) onto a histogram $R_{n\Delta t}$ which is almost uniform in $1 \leq l \leq P$. One such function can be constructed by mapping the mass corresponding to each value of the cumulative distribution function (cdf) of (47), onto an equal mass on the uniform distribution over the P processors. In another implementation of the mass transport method we can adjust the size of the coarse cells C_m according to the workload redistribution strategy discussed earlier, see Figure 3. This is effectively a one-dimensional example of an adsorption/desorption process where the mass transport procedure is carried out by mapping (47) into a new histogram $R_{n\Delta t}(\sigma) = R_{n\Delta t}(l; \sigma)$ corresponding to a new set of variable size coarse cells C_l , $1 \leq l \leq M'$. The cell size adjustment ensures the uniformity of the new histogram by defining $R_{n\Delta t}$ as a mapping of the cdf corresponding to (47).

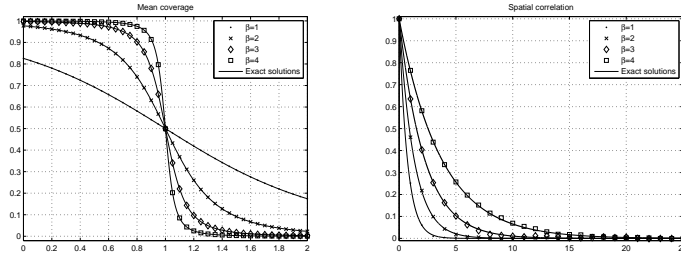
The mass transport mappings discussed above are not expected to be carried out at every time step $n\Delta t$ in order to reduce computational and communication cost, but instead they should follow a rationally designed coarser-in-time schedule, in analogy to processor communication scheduling, e.g., (20). The overall implementation appears rather simple since here we demonstrated the methodology in a one-dimensional example. However, in higher dimensions, adjusting the size and shape of coarse cells C_m can be much harder. Nevertheless the structure of re-balancing procedure can remain one-dimensional even in higher dimensional lattices if we pick a sub-lattice decomposition (5) into strips C_m . We note that the mapping we constructed using cdf's did not take into account the processor architecture and a suitable cost functional formulation for the mass transport to a uniform distribution, as in the Monge-Kantorovich problem, [10], may be more appropriate. We will revisit such issues in a future publication.

7. Parallel Simulations: Benchmarks and Applications

Exactly solvable models of statistical mechanics provide a test bed for sampling algorithms applied to interacting particle systems. We present benchmarks for two important cases: (a) sampling of equilibrium distributions, i.e., long time behavior of the simulated Markov process, and (b) weak approximations of the dynamics. In the first set of tests we work with the classical Ising model on one and two dimensional lattices where spins interact through a nearest-neighbor potential. Thus the Hamiltonian of the system is

$$H(\sigma) = -\frac{K}{2} \sum_{x \in \Lambda_N} \sum_{|y-x|=1} \sigma(x)\sigma(y) + h \sum_{x \in \Lambda_N} \sigma(x),$$

where K is a real parameter that defines the strength of the interaction and h the external field. We work with the spin-flip Arrhenius dynamics with the rates defined in the nearest-neighbor set $\Omega_x = \{z \mid |z - x| = 1\}$ and the updates



(a) Coverage

(b) Two-point spatial correlations

Figure 4: (a) Comparison of the exact solution (51) (solid line) for the total coverage $c_\beta(K, h)$, $K = 1$, with the mean coverage obtained in simulations on the one-dimensional lattice with $N = 2^{15}$ and $\Delta t = 1.0$. (b) Two-point spatial correlation function estimated at $h = 1$ on the same lattice and $\Delta t = 1.0$ compared to the exact solution.

in $\mathcal{S}_x = \{0, 1\}$.

$$c(x, \sigma) = c_1(1 - \sigma(x)) + c_2\sigma(x)e^{-\beta U(x)}, \quad (48)$$

$$U(x) = K \sum_{y \in \Omega_x} \sigma(x + y) + h, \quad (49)$$

with β is a given inverse temperature. The generator of (48) is a self-adjoint operator on the space $L^2(\mathcal{S}, \mu_N)$ where $\mu_N(d\sigma) = Z^{-1}e^{-\beta H(\sigma)} d\sigma$ is the canonical Gibbs measure of the system at the constant inverse temperature β . Consequently the dynamics is reversible and the measure μ_t of the process $\{S_t\}_{t \geq 0}$ converges to the Gibbs measure μ_N as $t \rightarrow \infty$. Thus the dynamics (48) can be used for computing expected values $\mathbb{E}_{\mu_N}[f]$ by invoking ergodicity and averaging on a single trajectory

$$\mathbb{E}_{\mu_N}[f] \equiv \int_{\mathcal{S}} f(\sigma) \mu_N(d\sigma) = \lim_{T \rightarrow \infty} \frac{1}{T} \int_0^T f(S_t) dt.$$

In the simulations we estimate two observables:

$$\text{mean coverage: } \bar{c}_t = \frac{1}{|\Lambda_N|} \mathbb{E} \left[\sum_{x \in \Lambda_N} \sigma_t(x) \right],$$

$$\text{2-point correlation function: } \bar{\lambda}_t(x, y) = \mathbb{E}[\sigma_t(x)\sigma_t(x + y)].$$

Due to translational invariance the function $\bar{\lambda}_k(x, y)$ depends on the distance $|x - y|$ only. For exactly solvable one and two dimensional Ising models we have explicit formulas which we summarize here for the spins in $\Sigma = \{0, 1\}$.

1D Ising model: The one-dimensional Ising model does not exhibit a phase transition and thus presents a simple benchmark for accuracy. Working with lattice gas models requires a simple transformation of the well-known exact solution, [5], which for the Hamiltonian of the system given on the periodic

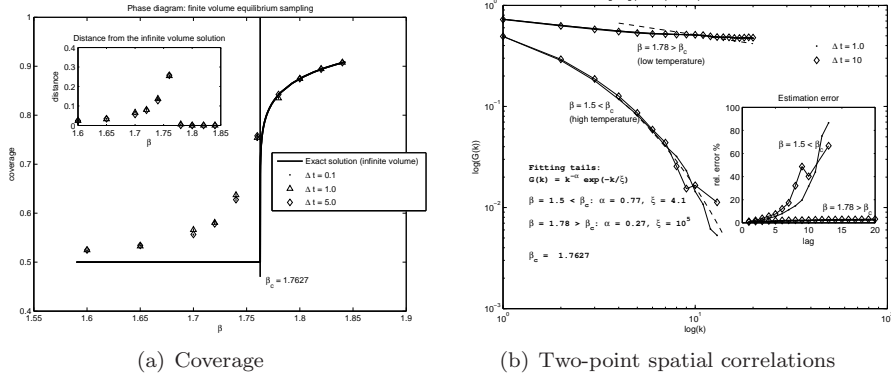


Figure 5: (a) Comparison of the exact solution (54) (solid line) for the total coverage $c_\beta(K, h)$, $h = 2$, with mean coverage obtained in simulations on the one-dimensional lattice with $N = 128$ and various Δt 's. (b) Spatial two-point correlation function in the two-dimensional Ising model simulated on the lattice $N = 512^2$ at a sub-critical temperature $\beta > \beta_c$ and supercritical regime $\beta < \beta_c$. The simulation confirms the behavior obtained from the infinite volume exact solution: at high temperatures the decay is exponential while at temperatures below the critical temperature the decay is algebraic. The dashed line represents the fitted function of the form $k^{-\alpha} e^{-k/\xi}$.

lattice

$$H(\sigma) = -K \sum_{x=1}^N \sigma(x)\sigma(x+1) + h \sum_{x=1}^N \sigma(x),$$

yields the equilibrium mean coverage and the 2-point correlation function

$$\bar{c}(h, \beta) = \frac{1}{2} \left(1 + \frac{\sinh(h')}{(\sinh^2(h') + e^{-4K'})^{1/2}} \right), \quad (50)$$

$$\bar{\lambda}(x, y) = \frac{1}{4} \left(1 + e^{4K'} \sinh^2(h') \right) \times \quad (51)$$

$$\left[\frac{e^{K'} \cosh(h') - e^{-K'} \left(1 + e^{4K'} \sinh^2(h') \right)^{1/2}}{e^{K'} \cosh(h') + e^{-K'} \left(1 + e^{4K'} \sinh^2(h') \right)^{1/2}} \right]^{(x-y)}, \quad y \geq x, \quad (52)$$

where

$$K' = \frac{1}{4}\beta K, \quad \text{and} \quad h' = \frac{1}{2}\beta(h - K). \quad (53)$$

Since the one-dimensional Ising model does not exhibit a phase transition it allows us to assess the accuracy of the approximation for the phase diagram calculation. The phase diagram depicting dependence of the coverage on the external field for different values of β is shown in Figure 4(a). In this simulation a rather conservative $\Delta t = 1.0$ was chosen. The statistical errors (confidence intervals) are below the resolution of the graph. As seen in the figure the isotherms

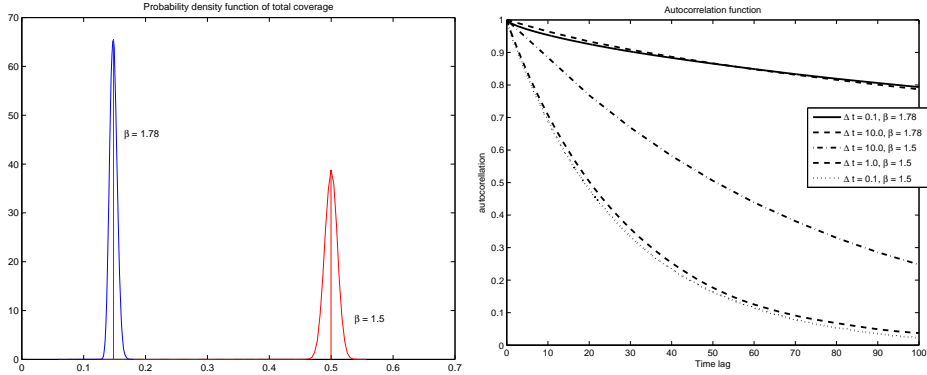


Figure 6: (a) Estimated equilibrium distributions of the coverage process at the two temperatures simulated in Fig. 5(b). (b) Autocorrelation functions for the coverage process in the two-dimensional Ising model simulated at $\beta = 1.5$ (high temperature above the critical temperature β_c and at $\beta = 1.78 > \beta_c$ (low temperature), see parameters in Fig. 5(b).

for the average equilibrium coverage are thus obtained with a good accuracy. As a global observable the total coverage is less sensitive to statistical errors therefore we also monitor the 2-point correlation function and its agreement with the exact solution (52). The results for different values of β in Figure 4(b) demonstrate good accuracy.

2D Ising model: The phase transition that occurs in two-dimensional Ising model presents a more challenging test case. However, the celebrated exact solution due to Onsager for spins $\Sigma = \{-1, 1\}$, [29], in the case with the zero external field and further refinements yield closed formulas for the mean coverage and two point correlation functions. We restrict our tests to the isotropic case, i.e., on the two-dimensional periodic lattice we have the Hamiltonian

$$H(\sigma) = -K \sum_{x=(x_1, x_2) \in \Lambda_N} (\sigma(x_1, x_2)\sigma(x_1, x_2 + 1) + \sigma(x_1, x_2)\sigma(x_1 + 1, x_2)) + h \sum_{x \in \Lambda_N} \sigma(x).$$

Transforming the exact solutions for the spins $\Sigma = \{0, 1\}$ we obtain the equivalent to the zero external field the value $h = 2K$ at which value the critical inverse temperature solves $\sinh(\frac{1}{2}\beta_c K) = 1$. The exact solution for the mean coverage has the form

$$\bar{c}(\beta) = \begin{cases} \frac{1}{2} \left(1 + [1 - (\sinh(\frac{1}{2}\beta K))^{-4}]^{1/8} \right), & \beta > \beta_c, \\ \frac{1}{2}, & \beta < \beta_c. \end{cases} \quad (54)$$

The exact solution for the 2-point correlation is available in [37], however, we

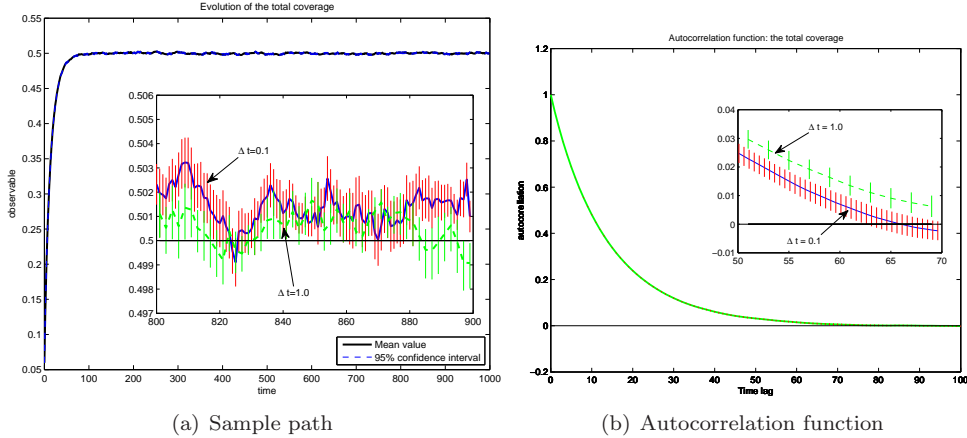


Figure 7: (a) A sample path of the total coverage process $\{S_t\}$ simulated at $\Delta t = 1.0$ and $\Delta t = 0.1$ on the one-dimensional lattice with $N = 2^{15}$ and $\Delta t = 1.0$. (b) Autocorrelation function of the coverage process. The means were obtained from $M = 1000$ independent realizations of the process at $\beta = 4$ and $h = 1$. The inset shows error bars for the empirical mean estimator.

use only the asymptotics in $|x - y|$, [5]. Introducing $\kappa = (\sinh(\frac{1}{2}\beta K))^{-2}$ we have

$$\bar{\lambda}(x, y) = \begin{cases} (1 - \kappa^2)^{1/4} + \mathcal{O}(\kappa^{|x-y|}), & \beta > \beta_c, \\ \mathcal{O}(\kappa^{-|x-y|/2}), & \beta < \beta_c. \end{cases} \quad (55)$$

The phase diagram is computed at $h = 2$ which for $K = 1$ corresponds to the regime when the second-order phase transition occurs at the critical temperature $\sinh(\frac{1}{2}K\beta_c) = 1$. Sampling the coverage exhibits well-known difficulties close to the critical point β_c which are not cured by the fractional step algorithm. Instead, we demonstrate in Figure 5(a) that for wide range of choices Δt the phase diagram is constructed accurately for β outside a neighborhood of β_c . Close to the critical point the algorithm provides approximations that are in agreement with other Monte Carlo sampling approach. The finite-size effects are pronounced at the neighborhood of the critical point due to algebraic decay of correlations. Thus it is not expected that a good agreement with the infinite volume exact solution will be observed in the finite size simulations. Nonetheless, the presence of the second-order phase transition is indicated in the computed phase diagram. Furthermore, the proposed algorithm provides an efficient implementation that allows for simulations on large lattice. It is shown in Figure 5(b) that algebraic decay of the 2-point correlation function is well approximated in the low-temperature (sub-critical) regime, while at super-critical temperatures the exponential decay is observed. Overall, we note that such long-time sampling of the simulated CTMC is a particularly challenging task since in principle, errors from any approximation may accumulate at long times and contaminate the simulation.

Table 1: An Event in Ω_x , $x^{nn} \in \Omega_x$ is a randomly selected site from the nearest-neighbor set of x , and $r_2(x) = \frac{1}{4}(1 - \sigma(x)^2)\nu_0^x$, $r_3(x) = \frac{1}{8}\sigma(x)(1 + \sigma(x))\nu_{-1}^x$, $r_4(x) = \frac{1}{8}\sigma(x)(\sigma(x) - 1)\nu_1^x$, where ν_k^x is the number of nearest neighbors (n.n.) of x that are equal to k .

ω	site	$\sigma(x)$	σ^x	Rate $c(x, \omega; \sigma)$	Comment
1	vacant	0	$0 \rightarrow 1$	$k_1(1 - (\sigma(x))^2)$	CO adsorb
2	vacant	0	$0 \rightarrow -1$ $0 \rightarrow -1, x^{nn}$	$(1 - k_1)r_2(x)$	O ₂ adsorb
3	CO	1	$1 \rightarrow 0$ $-1 \rightarrow 0, x^{nn}$	$k_2r_3(x)$	CO + O and desorb
4	O	-1	$-1 \rightarrow 0$ $1 \rightarrow 0, x^{nn}$	$k_2r_4(x)$	CO + O and desorb

Studying approximation properties of the stochastic dynamics poses a more difficult task due to the lack of an exact solution for the evolution of observables. Certain guidance can be obtained from mean-field approximations, however, those do not give sufficiently good approximation for Ising model in low dimensions. Therefore we compare the evolution of the coverage obtained from the traditional SSA algorithm with approximations generated by the proposed fractional time step algorithm with different choices Δt . In Figure 7(a) we compare the expected value and variance of the total coverage process $C_t = \frac{1}{|\Lambda_N|} \sum_{\Lambda_N} S_t(x)$. Furthermore, it is also shown that the auto-correlation function for the process C_t is well-approximated and approximations converge as $\Delta t \rightarrow 0$, see Figures 7(b) and 6(b).

7.1. Examples from Catalysis and Reaction Engineering

In order to demonstrate the applicability of the proposed parallelization methodology in systems exhibiting complex spatio-temporal morphologies at mesoscopic length scales, e.g., islands, spirals, rings, etc., we implement a KMC algorithm arising in the modeling of chemical reaction dynamics on a catalytic surface. Here we focus on CO oxidation, which is a prototypical example for molecular-level reaction-diffusion mechanisms between adsorbates on a surface. We note that molecular dynamics simulations have also been employed to understand micro-mechanisms on surfaces such as reaction paths [30]. However, reaction kinetics for mesoscale adsorbate structures cannot be simulated by using molecular dynamics because of spatio-temporal scale limitations of such methods, while KMC methods, have the ability to simulate much larger scales [23].

In KMC models for CO oxidation on a catalytic surface spatial resolution is a critical ingredient of the modeling since in-homogeneously adsorbed O and CO react on the catalytic surface only where the corresponding phases meet. Sophisticated KMC models for CO oxidation on catalytic surfaces, where kinetic parameters are estimated by *ab initio* density functional theory (DFT), [16], were recently developed in [31] and later in [27], [21]. Such KMC models yield

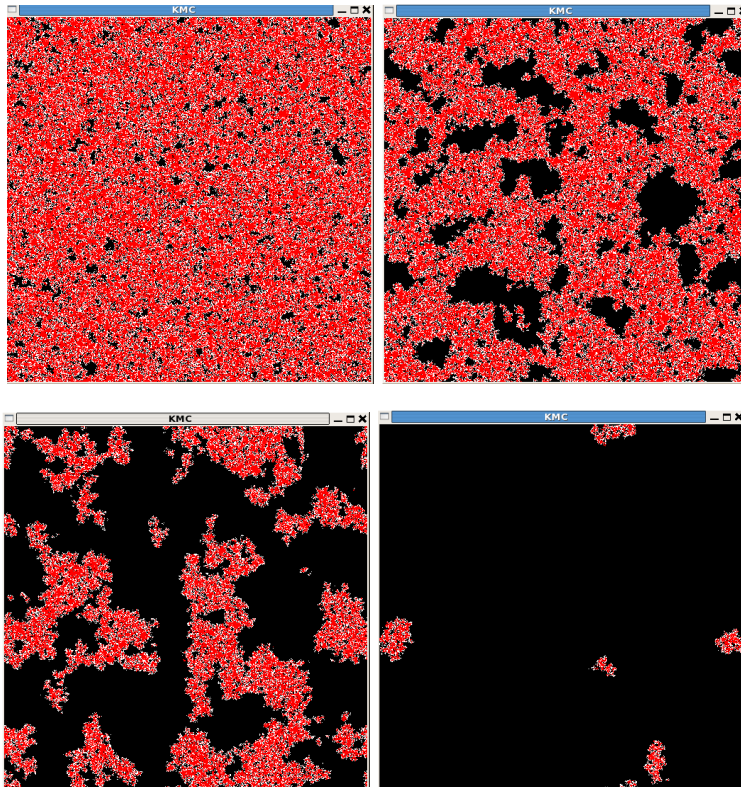


Figure 8: Snapshot at different simulation times for the CO oxidation process, on a two-dimensional lattice $N = 1024^2$.

a remarkable agreement with experiments, see also the review articles [26] and [8].

Next we demonstrate the performance of parallel Fractional Step algorithms for KMC simulation to heterogeneous catalysis. We implement a simplified CO oxidation model known as the Ziff-Gulari-Barshad (ZGB) model, [39], which was one of the first attempts towards a spatially distributed KMC modeling in reaction systems. Although a simplified model compared to the *ab initio* KMC models described earlier, it incorporates the basic mechanisms for the dynamics of adsorbate structures during CO oxidation on catalytic surfaces: single site updates (adsorption/desorption) and multi-site updates (specifically, reactions with two sites being involved). The spins take values $\sigma(x) = 0$ denoting a vacant site $x \in \Lambda_N$, $\sigma(x) = -1$ for a molecule CO at x , and $\sigma(x) = 1$ representing a O_2 molecule. Depending on the local configurations of the nearest neighbors in $\Sigma_x = \{y \mid |y-x| = 1\}$ the events in Table 1 are executed. The rates of individual events depend on the states in Ω_x which are enumerated by $\omega = \{1, 2, 3, 4\}$ and are summarized in Table 1.

The execution times for lattices of different sizes are compared in Figure 2,

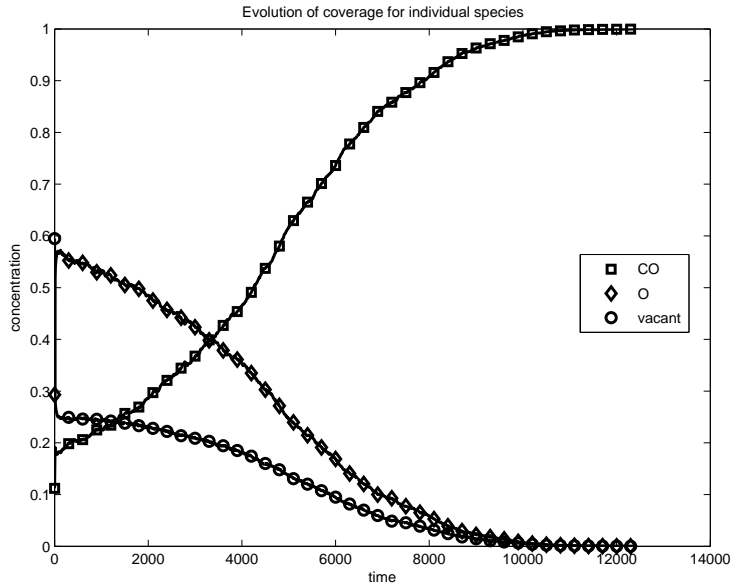


Figure 9: Evolution of the mean coverage for species in the oxidation process (CO, O₂, and vacant sites).

while a snapshot of the spatial morphology is depicted in Figure 8. Here we take as a reference the sequential KMC-BKL kernel. The same kernel is then used for the implementation on GPUs where we compare times for different choices of Δt . We remark that the KMC kernel is not optimized by techniques such as the BKL algorithm, [19], which is manifested in the scaling with respect to the size of the lattice N . However, the *same kernel* is used in the fractional step algorithm thus we present fair comparisons between serial and parallel solvers, noting that any optimized serial KMC algorithm can be used as a kernel in our Fractional Step framework. It is worth noting that by partitioning of the problem into the subproblems the $\mathcal{O}(N^2)$ complexity of the simple implementation for the SSA algorithm is reduced, which is also demonstrated in Figure 2 where the slope of lines for simulations using GPUs suggest the reduced complexity of order $\mathcal{O}(N)$. Hence the proposed approach also offers a simple but efficient implementation of KMC simulators.

Finally, in our implementation (as well as in the original ZGB model) we did not implement the fast diffusion mechanism of O adsorbates on the surface, [21]. However, the scheme (16) can allow us to easily implement within our parallelization framework schemes with disparate time-scales which turn out to be important for the long-time adsorbate dynamics.

8. Conclusions

In this paper we proposed a new framework for constructing parallel algorithms for lattice KMC simulations. Our approach relies on a spatial decomposition of the Markov generator underlying the KMC algorithm, into a hierarchy of operators corresponding to processors' structure in the parallel architecture. Based on this operator decomposition, we can formulate Fractional Step Approximation schemes by employing the Trotter product formula; these schemes allow us to run independently on each processor a serial KMC simulation on each fractional time-step window. Furthermore, the schemes incorporate the Communication Schedule between processors through the sequential application of the operators in the decomposition, as well as the time step employed in the particular fractional step scheme. Here we discussed deterministic schedules resulting from Lie- and Strang-type fractional step schemes, as well as random schedules derived by the Random Trotter Theorem, [18]. We demonstrated that the latter category includes the algorithm [34] as one particular example.

Some of the key features of the proposed framework and possible future directions include: The hierarchical structure can be easily derived and implemented for very general physiochemical processes modeled by lattice systems, allowing users to input as the KMC kernel their preferred serial algorithm. This flexibility and hierarchical structure allow for tailoring our framework to particular parallel architectures with complex memory and processor hierarchies, e.g., clusters of GPUs communicating, for instance, through an MPI protocol, and using the nested generator decomposition (46). Moreover, multi-scale Trotter algorithms for systems with fast and slow processes are widely used in Molecular Dynamics, e.g., [12], and they can be recast along with the proposed methods into a spatio-temporal hierarchy of operators that allow computational tasks to be hierarchically decomposed in space/time. The numerical consistency of the proposed algorithms is rigorously justified by Trotter Theorems, [36, 18] showing the convergence of our approximating schemes to the original serial KMC algorithm. Related numerical estimates are expected to provide insights on the design and the relative advantages of various communication schedules and architectures. We discussed work load balancing between processors through a re-balancing scheme based on probabilistic mass transport methods that is particularly well-suited for the proposed fractional step KMC methods. We carried out detailed benchmarking using analytically available exact solutions from statistical mechanics and applied the method to simulate complex spatially distributed molecular systems, such as reaction-diffusion processes on catalytic surfaces. Finally, we studied the performance and scalability of our algorithm (46) and the resulting code for different lattice sizes and types of GPUs.

Concluding we note that there are some interesting conceptual analogies between the parallelization and coarse-graining algorithms of KMC such as the Coarse-Grained Monte Carlo (CGMC) method e.g., [14, 2]. In both methods we decompose the particle system in components communicating minimally, e.g., (10), (12), or trivially as in coarse-graining methods, thus, local information is represented by collective (coarse) variables, or computed on separate processors

within a parallel architecture. An early work towards parallelizing CGMC [14] in problems with locally well-mixed particle interactions is [38], while further progress towards understanding and exploiting the analogies and the complementarity of CGMC and parallel KMC has the potential to give efficient KMC algorithms capable of simulating complex systems at mesoscopic length scales.

Acknowledgments: The research of M.A.K. was partially supported by the National Science Foundation under the grant NSF-DMS-071512, by the Office of Advanced Scientific Computing Research, U.S. Department of Energy under DE-SC0002339 and the European Commission FP7-REGPOT-2009-1 Award No 245749. The research of P.P. was partially supported by the National Science Foundation under the grant NSF-DMS-0813893 and by the Office of Advanced Scientific Computing Research, U.S. Department of Energy under DE-SC0001340; the work was partly done at the Oak Ridge National Laboratory, which is managed by UT-Battelle, LLC under Contract No. DE-AC05-00OR22725. The research of G.A. was partially supported by the National Science Foundation under the grant NSF-DMS-071512 and NSF-CMMI-0835582. The research of M. T. was partially supported by the AFOSR STTR Program, the Army Research Office under the grant 54723-CS, and the NVIDIA University Professor Partnership Program. The research of L.X. was supported by the National Science Foundation under the grant NSF-DMS-0813893.

References

- [1] G. Arampatzis, M.A. Katsoulakis, P. Plecháč, L. Rey-Bellet, Error analysis for parallel kinetic monte carlo algorithms: accuracy and processor communication, 2011. Preprint.
- [2] S. Are, M.A. Katsoulakis, P. Plecháč, L. Rey-Bellet, Multibody interactions in coarse-graining schemes for extended systems, *SIAM J. Sci. Comput.* 31 (2008) 987–1015.
- [3] S.M. Auerbach, Theory and simulation of jump dynamics, diffusion and phase equilibrium in nanopores., *Int. Rev. Phys. Chem.* 19 (2000).
- [4] S.P.C. Battaile, M. Chandross, L. Holm, A. Thompson, V. Tikare, G. Wagner, E. Webb, X. Zhou, C.G. Cardona, A. Slepoy, Crossing the mesoscale no-man’s land via parallel kinetic Monte Carlo, Sandia report (2009).
- [5] R.J. Baxter, *Exactly Solved Models in Statistical Mechanics*, Academic Press, 3rd edition, 1989.
- [6] A.B. Bortz, M.H. Kalos, J.L. Lebowitz, A new algorithm for Monte Carlo simulation of Ising spin systems, *Journal of Computational Physics* 17 (1975) 10–18.
- [7] A. Chatterjee, D. Vlachos, An overview of spatial microscopic and accelerated kinetic Monte Carlo methods, *Journal of Computer-Aided Materials Design* 14 (2007) 253–308. 10.1007/s10820-006-9042-9.

- [8] C.H. Christensen, J.K. Norskov, A molecular view of heterogeneous catalysis, *Journal of Chemical Physics* 128 (2008).
- [9] S.G. Eick, A.G. Greenberg, B.D. Lubachevsky, A. Weiss, Synchronous relaxation for parallel simulations with applications to circuit-switched networks, *ACM Trans. Model. Comput. Simul.* 3 (1993) 287–314.
- [10] L.C. Evans, Partial differential equations and Monge-Kantorovich mass transfer, in: *Current developments in mathematics, 1997* (Cambridge, MA), Int. Press, Boston, MA, 1999, pp. 65–126.
- [11] D.T. Gillespie, A general method for numerically simulating the stochastic time evolution of coupled chemical reactions, *Journal of Computational Physics* 22 (1976) 403–434.
- [12] E. Hairer, C. Lubich, G. Wanner, Geometric numerical integration, volume 31 of *Springer Series in Computational Mathematics*, Springer-Verlag, Berlin, second edition, 2006. Structure-preserving algorithms for ordinary differential equations.
- [13] P. Heidelberger, D.M. Nicol, Conservative parallel simulation of continuous time Markov chains using uniformization, *IEEE Trans. Parallel Distrib. Syst.* 4 (1993) 906–921.
- [14] M. Katsoulakis, A. Majda, D. Vlachos, Coarse-grained stochastic processes for microscopic lattice systems, *Proc. Natl. Acad. Sci* 100 (2003) 782–782.
- [15] M.A. Katsoulakis, P. Plecháč, A. Sopasakis, Error analysis of coarse-graining for stochastic lattice dynamics, *SIAM J. Numer. Anal.* 44 (2006) 2270–2296.
- [16] W. Kohn, Nobel Lecture: Electronic structure of matter-wave functions and density functionals, *Reviews of Modern Physics* 71 (1999) 1253–1266.
- [17] G. Korniss, M.A. Novotny, P.A. Rikvold, Parallelization of a dynamic Monte Carlo algorithm: A partially rejection-free conservative approach, *Journal of Computational Physics* 153 (1999) 488–508.
- [18] T.G. Kurtz, A random Trotter product formula, *Proc. Amer. Math. Soc.* 35 (1972) 147–154.
- [19] D.P. Landau, K. Binder, A guide to Monte Carlo simulations in statistical physics, Cambridge University Press, Cambridge, 2000.
- [20] T.M. Liggett, Interacting Particle Systems, volume 276 of *Grundlehren der mathematischen Wissenschaften*, Springer-Verlag, New York, Berlin, Heidelberg, Tokyo, 1985.
- [21] D.J. Liu, J.W. Evans, Atomistic and multiscale modeling of CO-oxidation on Pd(100) and Rh(100): From nanoscale fluctuations to mesoscale reaction fronts, *Surf. Science* 603 (2009) 1706–1716.

- [22] B.D. Lubachevsky, Efficient parallel simulations of dynamic Ising spin systems, *J. Comput. Phys.* 75 (1988) 103–122.
- [23] J.J. Lukkien, J.P.L. Segers, P.A.J. Hilbers, R.J. Gelten, A.P.J. Jansen, Efficient Monte Carlo methods for the simulation of catalytic surface reactions, *Physical Review E* 58 (1998) 2598–2610.
- [24] E. Martínez, J. Marian, M.H. Kalos, J.M. Perlado, Synchronous parallel kinetic Monte Carlo for continuum diffusion-reaction systems, *J. Comput. Phys.* 227 (2008) 3804–3823.
- [25] M. Merrick, K.A. Fichthorn, Synchronous relaxation algorithm for parallel kinetic Monte Carlo simulations of thin film growth, *Phys. Rev. E* 75 (2007) 011606.
- [26] H. Metiu, Preface to special topic: A survey of some new developments in heterogeneous catalysis, *Journal of Chemical Physics* 128 (2008).
- [27] M. Nagasaka, H. Kondoh, I. Nakai, T. Ohta, CO oxidation reaction on Pt(111) studied by the dynamic Monte Carlo method including lateral interactions of adsorbates, *J. Chem. Phys.* 126 (2007) 044704–7.
- [28] G. Nandipati, Y. Shim, J.G. Amar, A. Karim, A. Kara, T.S. Rahman, O. Trushin, Parallel kinetic Monte Carlo simulations of Ag(111) island coarsening using a large database, *Journal of Physics Condensed Matter* 21 (2009) 084214.
- [29] L. Onsager, Crystal statistics. I. A two-dimensional model with an order-disorder transition, *Phys. Rev.* 65 (1944) 117–149.
- [30] M.C. Payne, M.P. Teter, D.C. Allan, T.A. Arias, J.D. Joannopoulos, Iterative minimization techniques for abinitio total-energy calculations - molecular-dynamics and conjugate gradients, *Reviews of Modern Physics* 64 (1992) 1045–1097.
- [31] K. Reuter, D. Frenkel, M. Scheffler, The steady state of heterogeneous catalysis, studied by first-principles statistical mechanics, *Physical Review Letters* 93 (2004).
- [32] J. Sanders, E. Kandrot, *CUDA by Example: An Introduction to General-Purpose GPU Programming*, Addison-Wesley Professional, Cambridge, 2010.
- [33] Y. Shim, J.G. Amar, Rigorous synchronous relaxation algorithm for parallel kinetic Monte Carlo simulations of thin film growth, *Phys. Rev. B* 71 (2005) 115436.
- [34] Y. Shim, J.G. Amar, Semirigorous synchronous relaxation algorithm for parallel kinetic Monte Carlo simulations of thin film growth, *Phys. Rev. B* 71 (2005) 125432.

- [35] G. Szabo, G. Fath, Evolutionary games on graphs, *Physics Reports* 446 (2007) 97–216.
- [36] H.F. Trotter, On the product of semi-groups of operators, *Proc. Amer. Math. Soc.* 10 (1959) 545–551.
- [37] T.T. Wu, B.M. McCoy, C.A. Tracy, E. Barouch, Spin-spin correlation functions for the two-dimensional Ising model: Exact theory in the scaling region, *Phys. Rev. B* 13 (1976) 316–374.
- [38] L. Xu, M. Taufer, S. Collins, D.G.P. Vlachos, Parallelization of Tau-Leap Coarse-Grained Monte Carlo Simulations on GPUs, in: *Proceedings of the 2010 IEEE/ACM International Parallel and Distributed Processing, International Parallel and Distributed Processing Symposium (IPDPS)*, , in press, 2010.
- [39] R.M. Ziff, E. Gulari, Y. Barshad, Kinetic phase transitions in an irreversible surface-reaction model, *Phys. Rev. Lett.* 56 (1986) 2553.